ACS chemical biology

ARTICLES

pubs.acs.org/acschemicalbiology

Fluorescence and Atomic Force Microscopy Imaging of Wall Teichoic Acids in *Lactobacillus plantarum*

Guillaume Andre,[†,#] Marie Deghorain,[‡,#] Peter A. Bron,[§,∥,⊥] Iris I. van Swam,[§,∥] Michiel Kleerebezem,[§,∥,¶] Pascal Hols,[‡,*] and Yves F. Dufrêne[†,*]

[†]Institute of Condensed Matter and Nanosciences — Bio & Soft Matter, Université catholique de Louvain, Croix du Sud 2/18, B-1348 Louvain-la-Neuve, Belgium

[‡]Institute of Life Sciences — Biochemistry and Molecular Genetics of Bacteria, Université catholique de Louvain, Croix du Sud 5/6, B-1348 Louvain-la-Neuve, Belgium

[§]Top Institute Food and Nutrition, PO Box 557, 6700 AN Wageningen, The Netherlands

[∥]NIZO food research BV, P.O. Box 20, 6710 BA Ede, The Netherlands

[⊥]Kluyver Centre for Genomics of Industrial Fermentation, Julianalaan 67, 2628 BC Delft, The Netherlands

[¶]Laboratory of Microbiology, Agrotechnology and Food Sciences, Wageningen University, Dreijenplein 10, 6703 HB, Wageningen, The Netherlands

Supporting Information

ABSTRACT: Although teichoic acids are major constituents of bacterial cell walls, little is known about the relationships between their spatial localization and their functional roles. Here, we used single-molecule atomic force microscopy (AFM) combined with fluorescence microscopy to image the distribution of wall teichoic acids (WTAs) in *Lactobacillus plantarum*, in relation with their physiological roles. Phenotype analysis of the wild-type strain and of mutant strains deficient for the synthesis of WTAs (Δ*tagO*) or cell wall polysaccharides (Δ*cps1-4*) revealed that WTAs are required for proper cell elongation and cell division. Nanoscale imaging by AFM showed that strains expressing WTAs have a highly polarized surface morphology, the poles being much smoother than the side walls. AFM and fluorescence imaging with specific lectin probes demonstrated that the polarized surface structure correlates with a heterogeneous distribution of WTAs, the latter being absent from the surface of the poles. These observations indicate that the polarized distribution of WTAs in *L. plantarum* plays a key role in controlling cell morphogenesis (surface roughness, cell shape, elongation, and division).

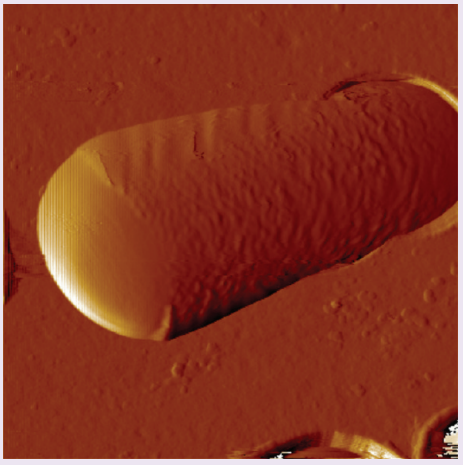

Lactic acid bacteria (LAB) play a central role in fermentations and are attracting considerable attention in view of their application as health-promoting cultures or probiotics.[1] *Lactobacillus plantarum*, one of the natural inhabitants of the human and animal gastrointestinal tract,[2] is a promising candidate probiotic species in view of its ability to survive several days in the human gastrointestinal tract,[3] and to adhere to human mucosa *in vitro*.[4]

Teichoic acids (TAs) and related glycopolymers represent a major class of cell wall constituents in Gram-positive bacteria, accounting for up to half of the weight of the cell wall.[5−7] TAs were initially discovered in bacterial extracts from the lactic acid bacterium *Lactobacillus arabinosus*,[8] currently renamed *L. plantarum*. The TA backbone generally consists of a poly(alditol phosphate) containing either glycerol or ribitol. As observed in most Gram-positive bacteria, *L. plantarum* contains two types of TAs, *i.e.*, lipo- and wall-teichoic acids (LTA and WTA, respectively). In *L. plantarum*, LTAs are polyglycerophosphate polymers mainly substituted with D-alanyl esters[9] and attached to the cytoplasmic membrane. WTAs are covalently bound to peptidoglycan (PG). In *L. plantarum*, two types of WTAs were found, based either on glycerol or ribitol depending on the strain.[10] Polyribitol- and polyglycerophosphate chains of WTAs are decorated by D-alanine esters and glucose substitutions.[10,11] Biosynthesis of WTA and LTA involves distinct biochemical pathways. WTA synthesis is controlled by specialized genes called *tag* or *tar* genes for the formation and export of polyglycerolphosphates or polyribitolphosphates, respectively. LTA biosynthesis is less characterized but involves the LTA-synthase LtaS, as a key enzyme that catalyzes the formation of polyglycerophosphates

Received: November 2, 2010
Accepted: January 10, 2011
Published: January 11, 2011

and was initially discovered in *Staphylococcus aureus* and in *Bacillus subtilis* (4 paralogues).[12−14]

Although WTAs and LTAs were originally thought to be essential for cell viability, WTA depletion was recently achieved in *B. subtilis* and *S. aureus* through the inactivation of the *tagO* gene that encodes the first enzyme in the WTA biosynthesis pathway.[15−17] In addition, mutants deficient for the LtaS synthase, and therefore lacking LTA synthesis, were shown to be viable in the same two species.[12,14,18] Nevertheless, both WTA- and LTA-deficient strains are strongly affected in cell morphology (*e.g.*, shape anomalies, aberrant septation), and combination of the two deficiencies appeared to be lethal, showing that the synthesis of anionic polymers is essential for cell physiology and survival.[12,14,18] As anionic polymers, TAs play a role as scavengers of cations such as Mg^{2+} and may create a pH gradient across the cell wall by sequestering the protons expelled through the cytoplasmic membrane in the generation of proton motive force.[19,20] This may influence the activity of several enzymes, in particular those involved in cell growth and division such as PG synthesizing machineries and/or PG hydrolases.[14,21−23] Notably, in *B. subtilis*, WTAs and LTAs appear to play distinct roles in morphogenesis, where WTA is required for proper cell elongation and LTAs for proper cell division.[14]

Although the chemical composition and biosynthesis of TAs are partially described, the three-dimensional organization of the individual molecules remains mysterious. Addressing this issue is an important step toward understanding the physiological roles of these polymers. Here, we use the combination of single-molecule atomic force microscopy (AFM) and fluorescence imaging to explore the spatial arrangement of WTAs in living *L. plantarum* cells. Using concanavalin A (ConA) lectin probes, we localize WTAs in the cell wall of wild-type (WT) and mutant cells impaired in the production of WTAs or cell wall polysaccharides (CPSs). The results show that the localization of WTAs in *L. plantarum* is highly heterogeneous and that this polarized distribution plays a key role in controlling cell morphogenesis (surface roughness, cell shape, elongation, and division). Our data provide new insights into the fate and functionality of WTAs during the cell cycle of *L. plantarum*.

RESULTS AND DISCUSSION

Inactivation of WTAs and CPS. Although WTAs are particularly abundant in *L. plantarum*,[10,11] little is known about their subcellular localization, organization, and function. To investigate the localization of WTAs in relation with their physiological role, we constructed a WTA-deficient derivative by mutation of the single *tagO* gene copy (Δ*tagO*) that encodes the first enzyme involved in WTA biosynthesis and has been shown to be dispensable in other species.[15,16] Besides TAs, the *L. plantarum* cell wall also contains polysaccharides (CPS) that could bind lectin probes, thereby interfering with the WTA localization. Therefore, a CPS^- null mutant was constructed as a control strain by deleting the four gene clusters potentially involved in CPS synthesis (Δ*cps1-4* strain, see Methods).

We confirmed that the two mutants indeed lack WTAs and CPS using X-ray photoelectron spectroscopy (XPS), a technique that analyses the chemical composition of the outermost cell surface.[24,25] Consistent with the general biochemical composition of bacterial cell walls, the main elements that were detected were C_{1s}, O_{1s}, and N_{1s} (Table 1). Phosphorus, which is abundant in TAs, was present in small amount in the WT (0.6%) but was hardly detected in the WTA-deficient strain. Compared to the WT, the phosphorus content in the CPS-deficient strain was clearly higher, consistent with the expectation that more TAs are surface-exposed when CPS have been removed. To gain a biomolecular view of the cell surface, the XPS data were converted into concentrations of basic model compounds,[26] *i.e.*, peptides, glycans, and lipids (Table 1). We found that the surface compositions of WT and WTA-deficient strains were very similar and consisted primarily of glycans with some peptides and lipids. By contrast, the CPS-deficient strain was poorer in glycans and much richer in peptides. Assuming that PG consists approximately of 50% glycans and 50% peptides,[26,27] we found that cell surface of the CPS-deficient strain is essentially composed of PG, together with proteins and TAs.

Table 1. Surface Chemical Composition of Three *L. plantarum* Strains Measured by XPS and Proportions of Carbon Involved in Peptides (C_{Pe}), Glycans (C_{Gl}), and Lipids (C_{Lp}) Deduced from the Data[a]

strain	% C	% O	% N	% P	% C_{Pe}	% C_{Gl}	% C_{Lp}
WT	60.0	36.5	2.3	0.6	14	68	18
WTA-deficient	60.5	36.4	2.8	0.1	16	66	18
CPS-deficient	59.9	28.4	9.7	1.4	59	34	7

[a] Mean of three independent experiments.

WTAs Are Required for Proper Cell Elongation and Division. We examined the growth and cell morphology of the WTA- and CPS-deficient strains in comparison with the WT strain. The WTA-deficient strain displayed a growth defect and reached a significantly lower final culture density compared to the WT (Supplementary Figure 1a). Light microscopy revealed that the growth defect of the WTA-deficient strain was associated with the presence of several morphological anomalies (Figure 1). First, WTA-deficient cells that were harvested in the exponential phase of growth displayed a tendency to remain associated in chains (65% of the cells compared to 35% in the WT, $n \geq 200$), indicating a defect in cell division and/or cell separation. Second, many cells were bent (46% of the cells, $n \geq 200$) and/or swollen. In addition, a statistical shape analysis showed that a high number of WTA-deficient cells were significantly shorter and/or displaying an increased diameter compared to WT cells (Supplementary Figure 1b and Supplementary Figure 1c). Third, FM4-64 staining of the plasma membrane revealed that a significant proportion (16%, $n \geq 200$) of cells contained displaced septa. The above morphological anomalies were even more pronounced in cells harvested from the stationary growth phase (Figure 1b), indicating that the absence of WTA disturbs cell elongation and division events. In contrast, similar analyses of the CPS-deficient strain did not reveal any major differences between this strain and the WT (Figure 1c). Altogether, these observations demonstrate that WTAs play an important role in controlling the morphogenesis of *L. plantarum* and highlight their requirement for proper cell elongation and division.

Polarized Surface Nanomorphology of *L. plantarum* Requires WTAs. Scanning electron microscopy of the WT strain suggested that the cell surface is homogeneous (Figure 2a). However, higher-resolution imaging by transmission electron microscopy (Figure 2b) and live cell imaging by AFM (Figure 2c−h) revealed a highly polarized cell envelope, the polar region being smoother than the side walls. Quantitative information on the cell surface roughness was obtained by performing statistical analysis of the AFM height images at various length scales. To

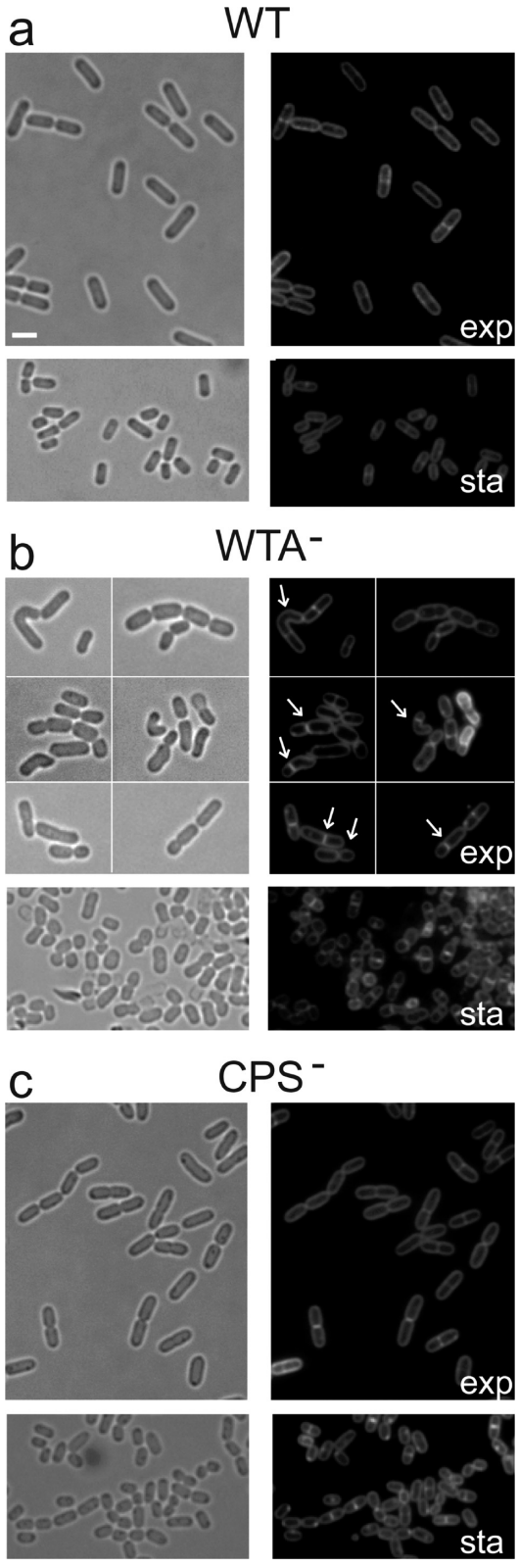

Figure 1. Phenotype analysis of *L. plantarum* WT and mutant cells. Bright-field (left) and fluorescence (right) images of (a) wild type (WT) cells, (b) WTA-deficient cells (WTA^-), and (c) CPS-deficient cells (CPS^-). For each strain, the upper panel shows exponentially growing cells, and the lower panel shows cells from the stationary phase. Arrows in the WTA-deficient strain indicate mispositioned septa and aberrant cell morphologies. Scale bar = 1 μm.

this end, surface roughness was analyzed through the power spectral density (PSD) of the fast Fourier transform of the height images.[28] Figure 2h shows the variation of root-mean-square roughness (Rr.m.s.) as a function of the length scale. The surface roughness of the poles increased very slightly with the length scale to reach a plateau at an Rr.m.s value of 0.7 ± 0.2 nm. By contrast, a much steeper increase of the Rr.m.s. was observed on the lateral region, yielding a plateau value of 3.7 ± 0.4 nm. Notably, the rough surface was decorated with waves 8 ± 3 nm in height and separated by 102 ± 12 nm. This peculiar morphology is not due to tip scanning artifacts since it was not affected by the scanning direction or the applied load and is reminiscent of the wave-like structures observed on another bacterium, *Lactobacillus rhamnosus* strain GG (LGG).[29] In the LGG case, the waves were attributed to extracellular polysaccharides (EPS), since they were no longer observed on a mutant impaired in EPS production.

The WT surface morphology characteristics were compared with those determined for WTA- and CPS-deficient strains (Figure 3). In contrast to WT cells, WTA-deficient cells displayed a rough, wave-like morphology over the entire surface and seemed to lack the smoother poles (Figure 3a−c). However, close examination revealed that, in WTA-deficient cells, the poles were slightly smoother than the side walls (Rr.m.s value at 500 nm of 2.5 ± 0.3 nm *vs* 4.7 ± 0.4 nm, respectively). In contrast, the surface morphology of CPS-deficient strain cells (Figure 3d−f) was highly polarized and very similar to that of WT cells (Rr.m.s value at 500 nm of 0.7 ± 0.2 and 3.5 ± 0.4 nm for the polar and lateral regions, respectively). These data indicate that the occurrence of proper cell morphogenesis and polarized surface morphology (smooth poles *vs* rough cell body) in *L. plantarum* are two phenotypical traits that require WTAs.

Localization of WTAs Using Fluorescence Microscopy. To investigate whether the shape anomalies and surface morphology of the different *L. plantarum* strains correlate with the localization of WTAs, the distribution of WTAs in the WT and WTA- and CPS-deficient strains was analyzed using fluorescence microscopy with a fluorescent ConA conjugate (Alexa Fluor 594 linked to succinylated ConA dimers) as a probe (Figure 4). The ConA lectin specifically binds glucose (or mannose) contained in glycopolymers and was used to label TAs in *S. aureus* and *B. subtilis*.[22,30,31] Since we previously showed that glucose substitutions of LTAs of *L. plantarum* WCFS1 were below the NMR detection threshold,[9] we expect that, among TAs, only the WTAs will be detected by the ConA probe. In addition, since glucose is included in the repetition unit of WTA without additional glucose decorations in *L. plantarum* WCFS1 (S. Tomita and S. Okada, Tokyo University of Agriculture, personal communication), the WTA backbone will be directly addressed. However, since CPS may also contain glucose (or mannose) residues, both WTA- and CPS-deficient strains were analyzed in order to distinguish the relative contributions of WTAs and CPS to the detection signal. All measurements were performed with cells collected from exponential and stationary phases of growth. Only data obtained in the exponential phase are presented, since they did not differ from those of the stationary phase.

WT cells were rarely labeled (around 10−15%). Fluorescence was observed all around the cells and was generally concentrated in cell aggregates (Figure 4a). As expected, cells treated with trichloroacetic acid (TCA), which removes PG-associated polymers, showed no labeling at all. Notably, the CPS-deficient strain showed substantial labeling (up to 45% of the cell population),

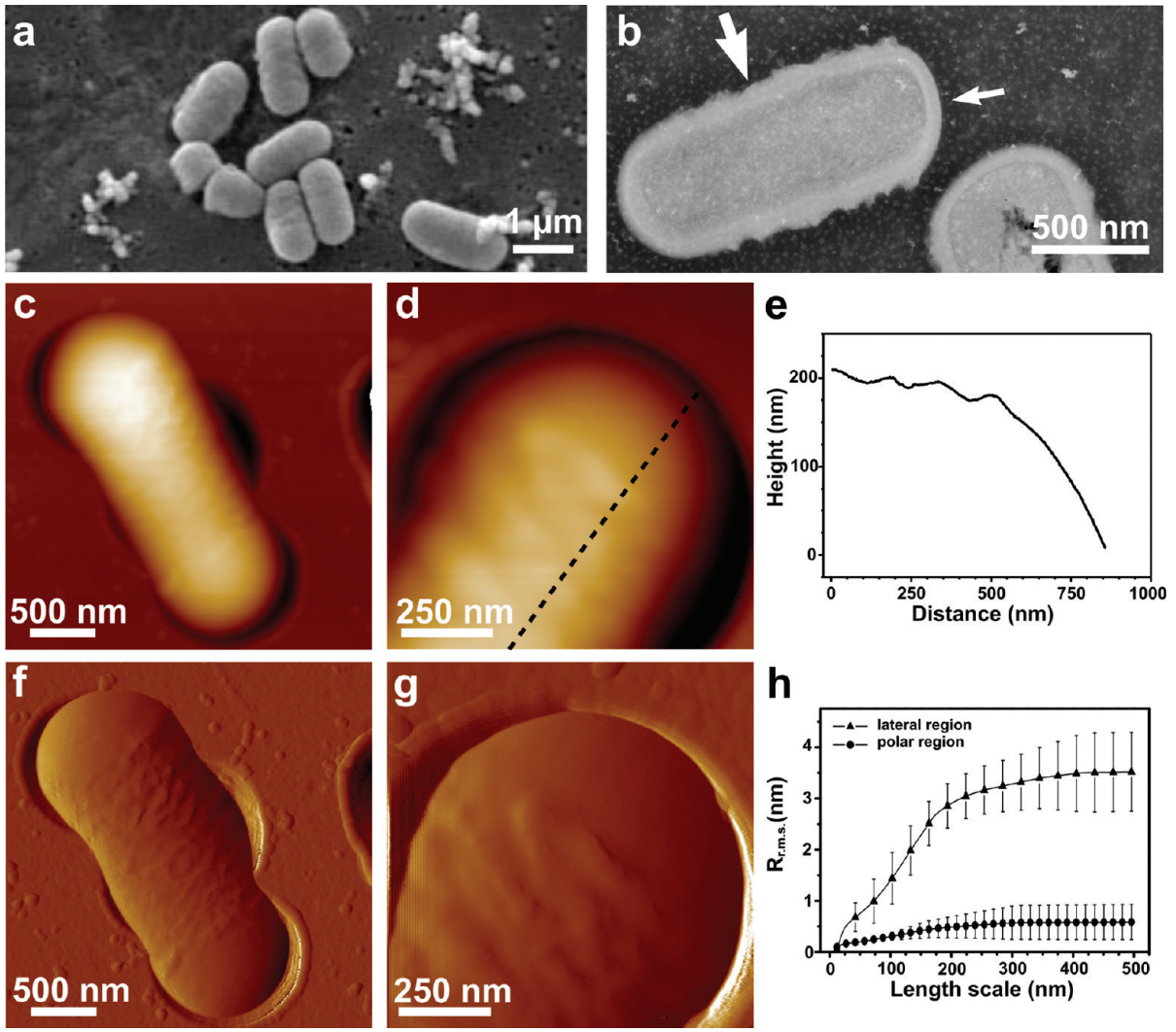

Figure 2. Electron microscopy and AFM topographic images of WT cells. (a) Scanning and (b) transmission electron microscopy images of *L. plantarum* WT cells. Transmission electron microscopy images suggest that the cell surface is polarized, the polar region (thin arrow) being smoother than the side walls (thick arrow). (c,d) Height and (f,g) deflection images of single *L. plantarum* WT cells in sodium acetate buffer, documenting a polarized surface morphology. (e) Vertical cross-section taken along the dotted line shown in panel d. (h) Variation of the root-mean-square roughness (Rr.m.s.) constructed from the power spectral density (PSD) analysis as a function of the length scale, on the smooth polar region (●) and on the rough lateral region (▲) of the cell. Each data point represents the mean ± standard deviation of 10 images obtained on 10 different cells.

thus revealing that the removal of CPS improved the ConA probe accessibility of glucose-based glycopolymers. Finally, the WTA-deficient strain displayed a complete lack of labeling except in aggregates of dead cells, indicating that WTAs were the main constituents detected by ConA.

The CPS-deficient cells exhibited heterogeneous staining patterns that were not observed in the WT, *i.e.*, fluorescent staining was absent from the septum region of dividing cells, as well as from the newly formed poles of the daughter cells (Figure 4b). This polar heterogeneity (new *vs* old pole) was no longer seen at a later stage of the reconstituted cell cycle, as indicated by fully labeled cells (Figure 4b and c). These observations indicate that (i) in CPS-deficient cells, WTAs could not be detected at the division site, and (ii) in WT cells, the polarized surface morphology and homogeneous fluorescent labeling are not correlated. We show below using single-molecule AFM that this apparent discrepancy is likely to result from the lack of sensitivity of the fluorescent probe.

Localization of WTAs Using Single-Molecule Force Spectroscopy. Whereas fluorescence imaging probes the entire cell wall, single-molecule force spectroscopy (SMFS) maps the distribution of single constituents on the outermost cell surface.[32−34] We therefore used SMFS with tips functionalized with ConA dimers to gain a more detailed view of the WTA surface distribution on the different strains. Figure 5a−c shows the adhesion force map (Figure 5a), the adhesion force histogram with representative force curves (Figure 5b), and the rupture length histogram (Figure 5c) recorded on the lateral region of WT cells. Adhesion forces of 69 ± 25 and 158 ± 45 pN mean magnitude were homogeneously distributed across the cell surface. In the light of earlier SMFS measurements,[29,35,36] we attribute these forces to the detection of single and double ConA-glucose interactions, reflecting the detection of one or two glycopolymer chains. Interestingly, the mean rupture distance was only 22 ± 11 nm (Figure 5c), suggesting that the stretched molecules were short and/or strongly anchored into the cell wall. Consistent

dx.doi.org/10.1021/cb1003509 |*ACS Chem. Biol.* 2011, 6, 366–376

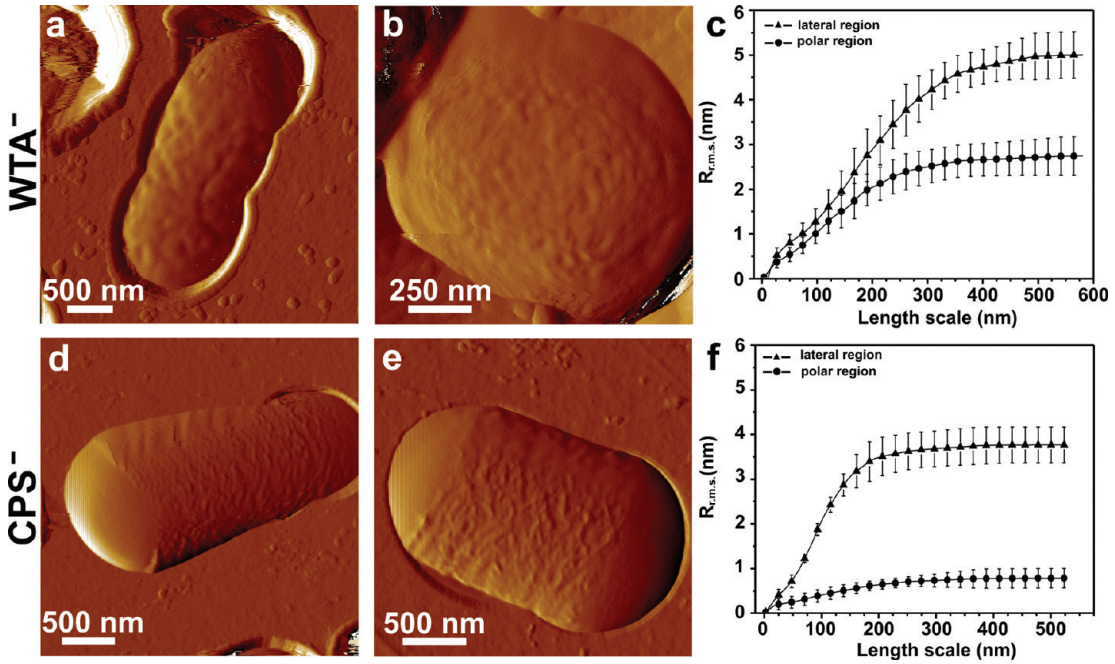

Figure 3. AFM topographic images of mutant cells. (a,b) Deflection images of single WTA-deficient cells (WTA^-) in sodium acetate buffer, documenting a rough morphology both on the (a) lateral and (b) polar regions. (d,e) Deflection images of single CPS-deficient cells (CPS^-) in sodium acetate buffer, revealing a polarized surface morphology. (c,f) Variation of the Rr.m.s. measured as a function of the length scale on the polar (●) and on the rough (▲) regions of the (c) WTA- and (f) CPS-deficient cells. Each data point represents the mean ± standard deviation of 8 images obtained on 8 different cells.

with this suggestion, most elongation force peaks could be fitted neither with the wormlike chain (WLC) model nor with an extended freely jointed chain (FJC+) model, which are typically used to describe the behavior of single protein and polysaccharide molecules, respectively.[36] These observations are in sharp contrast with results typically obtained for bacterial cell surface polysaccharides. For instance, force curves recorded on LGG bacteria with a ConA-tip displayed rupture lengths of up to 400 nm and were well-fitted with an FJC+ model.[29] This strongly suggests that the glycopolymers detected here reflect WTAs rather than other cell wall constituents. Based on the above findings, a 3-D view of the polymer properties was constructed by combining adhesion forces (false colors, yellow meaning larger adhesion forces) and rupture distances (z level) measured on every position (Figure 5c, inset). The map clearly documents the massive detection of single glycopolymers, presumably WTAs, on the lateral region of *L. plantarum*.

Notably, molecular recognition mapping of the poles revealed an almost complete lack of glucose residues (Figure 5d−f). In addition, large variations in rupture distances and adhesion forces were observed at the poles, which probably reflect nonspecific adhesion. These recognition data correlate with the structural images and demonstrate that the *L. plantarum* surface is highly polarized, the poles being much poorer in glucose-based glycopolymers than the rest of the cells. This heterogeneous composition was further confirmed by recording adhesion maps on the frontier region separating the pole from the side walls (Figure 5g−i).

Contrary to the WT strain, glucose-based glycopolymers were hardly detected on the cell surface of the WTA-deficient strain (Figure 6a−c), whatever the subcellular region investigated (polar region *vs* lateral region). Recognition maps obtained for the CPS-deficient strain (Figure 6d−i) were virtually identical to those obtained with the WT strain. These observations are consistent with the fluorescence data (Figure 4) and demonstrate that the glycopolymers detected on the WT surface reflect primarily WTAs.

Biological Implications and Concluding Remarks. AFM and fluorescence microscopy, combined with the use of specific cell wall mutants, provide a powerful approach for studying the organization of TAs in living Gram-positive bacteria. Whereas fluorescence microscopy localizes TAs in the entire cell wall with submicrometer resolution, AFM maps the distribution of single TA molecules on the outermost cell surface (Figure 7). We have shown that the localization of WTAs in *L. plantarum* is highly heterogeneous and that this heterogeneous distribution plays a key role in controlling cell morphogenesis. Our findings are consistent with the notion that the organization of many bacteria is highly polarized and that this cellular asymmetry is used to achieve functions.

Combined AFM and fluorescence imaging revealed the complex architecture and WTA distribution of the *L. plantarum* cell envelope (Figure 7a). Specifically, we showed that (i) WT cells have a highly polarized surface nanomorphology (smooth pole *vs* rough lateral region), which requires WTAs since WTA-deficient cells are no longer polarized; (ii) WTAs are largely absent from the surface of the poles, which correlates with the surface nanomorphology; (iii) WTAs are not detected at the division site (septum and newly formed poles) of the CPS-deficient strain; and (iv) with time, WTAs are progressively found at the poles during the cell cycle (Figure 7b). That WTAs were not detected in the septum region may reflect a lack of this component at this specific location. However, we cannot exclude other explanations, such as a lack of accessibility of WTAs at this site (packing or length of the polymers), a lack of specificity of the ConA probe, and the presence of immature forms of WTA.

dx.doi.org/10.1021/cb1003509 |*ACS Chem. Biol.* 2011, 6, 366–376

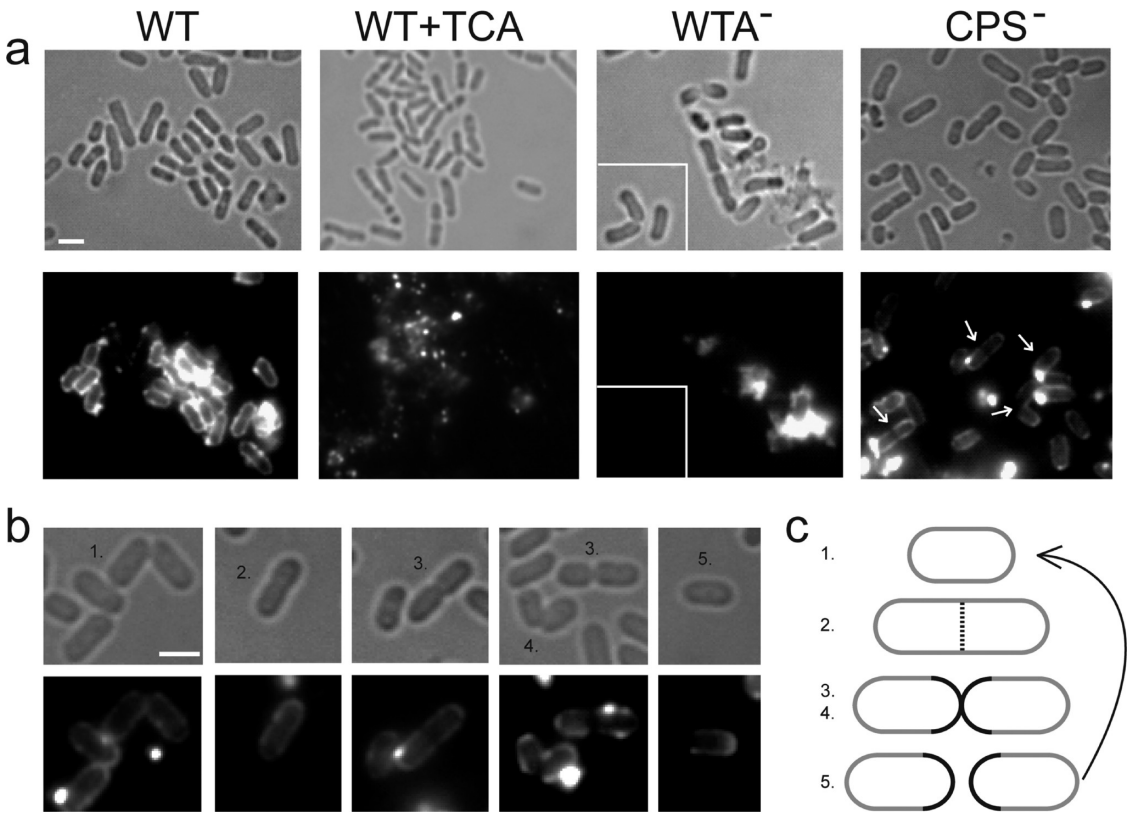

Figure 4. Fluorescence imaging of WTAs. (a) Phase contrast and fluorescence images of WT cells, TCA-treated WT cells, WTA-deficient cells (WTA^-), and CPS-deficient cells (CPS^-) stained with fluorescent ConA. Cells were harvested from the exponential phase. Arrows in the CPS-deficient strain indicate dark areas corresponding to the lack of fluorescence at the septum and new poles of the cells. Scale bar = 1 μm. (b) Selection of images obtained for the CPS-deficient strain at various stages of the cell cycle and (c) schemes of the proposed cell wall staining (numbers correspond to the different stages shown in panel b). Following division (stages 2−5), the two newly formed poles are depleted in WTAs, thus resulting in a lack of staining. The heterogeneity between the new and old poles is no longer observed at a later stage of growth (Stage 1). Scale bar = 1 μm.

Regarding the apparent discrepancy between fluorescence data (full labeling) and AFM data (lack of polar labeling) obtained on dividing cells, a possible explanation is that the fluorescent probe detects WTAs deeper in the cell wall, while the AFM probe addresses the extreme surface of the cell (Figure 7). According to the "inside to outside" PG assembly model,[37,38] its turnover is slower at the pole compared to the side walls, meaning that WTA-modified PG could remain localized in the layers close to the plasma membrane at the poles. This is consistent with our nanomorphology data obtained for WT and CPS-deficient cells, showing a surface layer attributed to WTAs only in the side walls.

The heterogeneous distribution of WTAs plays a key role in controlling cell morphogenesis since WTAs are required for proper cell elongation and division and for polarized surface morphology. A comparative study of WTA- and LTA-deficient strains in *B. subtilis* made it possible to assign distinct morphogenetic functions to WTAs and LTAs, the former being especially involved in cell elongation and the latter in cell division.[14] Here, cells of the WTA-deficient strain of *L. plantarum* were shown to be shorter and strongly affected in shape, similarly to the *tagO* mutant of *B. subtilis*.[14,15] Also, *L. plantarum* WTA-deficient cells were bent and/or swollen, suggesting that the control of cell morphometry along the longitudinal and cross-sectional axes is lost in the mutant. In contrast to WTA in *B. subtilis*,[14] *L. plantarum* WTA appeared to be important for proper cell division. WTA-deficient cells had displaced septa leading to asymmetric division, suggesting that subcellular recruitment of the cell division machinery is not properly coordinated and/or activated in the mutant. Taken together, our observations support the hypothesis that preventing WTA synthesis can locally disturb the cell wall composition, thereby altering the proper localization and/or activity of cell elongation and division machineries that are required for appropriate control of cell morphogenesis. Our findings are consistent with two recent studies in *S. aureus*.[39,40] The first report, by Atilano *et al.*,[39] provides a specific molecular mechanism for how WTAs may regulate PG biosynthesis by scaffolding *S. aureus* PBP4, its recruitment being mediated by immature forms of WTAs only present at the septum. More recently, Campbell *et al.*[40] provided evidence that WTAs play a fundamental role in regulating cell division in *S. aureus*. Cell division defects were observed when TarO is inactivated, suggesting that WTAs play a role in the regulation of PG biosynthesis by helping to assemble the cell division machinery.

We propose that the heterogeneous distribution of WTAs controls the location of PG hydrolases in *L. plantarum*, which in turn affects cell division. Recent studies have revealed heterogeneous WTA distributions (septum *vs* rest of the cell) in *B. subtilis*, *S. aureus*, and *S. pneumoniae*.[21−23,39,40] It has been suggested that the observed heterogeneity plays a key role in targeting PG hydrolases toward the site where they perform daughter cells separation after cell division. Consistent with these studies, the *L. plantarum* WTA-deficient strain displayed an increased tendency to remain associated in chains and increased cell lysis in the stationary phase of growth, suggesting that the activity or

dx.doi.org/10.1021/cb1003509 |*ACS Chem. Biol.* 2011, 6, 366–376

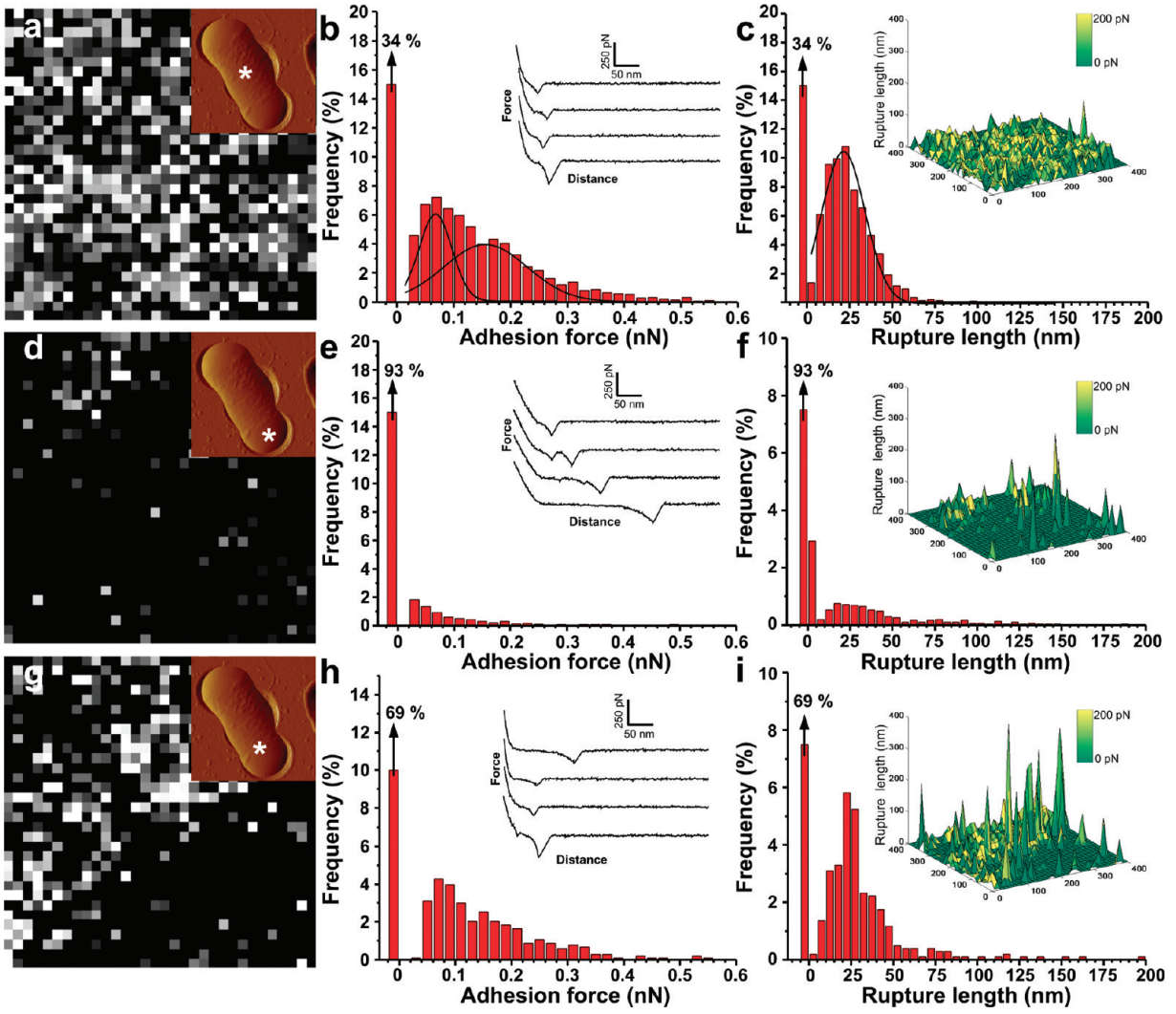

Figure 5. Single-molecule AFM imaging of WTAs in WT cells. (a,d) Adhesion force maps (400 × 400 nm, gray scale: 250 pN) recorded in buffer on the lateral and polar regions of *L. plantarum* WT cells using a ConA tip. Insets: deflection images in which the ∗ symbol indicates where the force maps were recorded. (b,e) Corresponding adhesion force histograms together with representative force curves. Each histogram was built from $n = 5120$ force curves from 5 maps, obtained using different tips and different cells. (c,f) Histograms of rupture distances ($n = 5120$) and representative 3-dimensional reconstructed maps obtained by combining adhesion force values (expressed as false colors) and rupture distances (expressed as z level) measured at different x, y locations. (g,h,i) Adhesion force map, adhesion force histogram, and rupture length histogram recorded on the frontier region separating the pole from the side walls.

location of PG hydrolases is affected by the lack of WTA. These observations suggest that WTAs also control the location of PG hydrolases in *L. plantarum*. Future studies using sublocalization experiments of PG hydrolases in both WT and WTA-deficient strains should help resolving the relationship between these PG degrading enzymes and WTA in *L. plantarum*.

METHODS

Bacterial Strains and Growth Conditions. *L. plantarum* WCFS1[41] and its derivatives were grown in Mann-Rogosa-Shape broth (MRS) (Difco) at 30 or 37 °C without agitation. *Escherichia coli* JM109 was used as an intermediate cloning host and cultivated aerobically at 37 °C in Luria−Bertani broth. When appropriate, antibiotics were added to the media. For *L. plantarum*, 10 μg/mL chloramphenicol and 10 μg/mL or (for replica plating) 30 μg/mL erythromycin were used. For *E. coli*, 10 μg/mL chloramphenicol and 250 μg/mL erythromycin were used.

DNA Manipulations. Plasmid DNA was isolated from *E. coli* using Jetstar columns as recommended by the manufacturer (Genomed GmbH, Bad Oberhausen, Germany). For DNA manipulations in *E. coli*, standard procedures were used.[42] Restriction endonucleases, DNA polymerases, and T4 DNA ligase were used as specified by the manufacturers (Promega, Leiden, The Netherlands; Boehringer, Mannheim, Germany). Primers were obtained from Genset Oligos (Paris, France).

Construction of Deletion Mutants. Construction of the *L. plantarum* gene deletion mutants for *tagO* (*lp_0730*) and *cps1-4* (*lp_2108* to *lp_2099* [*cps1*, *cps2*, and *cps3*] and *lp_1176* to *lp_1227* [*cps4*]) was performed as previously described.[43,44] A double crossover gene replacement strategy was used to replace the target gene(s) by a chloramphenicol resistance cassette (*lox66*-P_{32}*cat*-*lox71*[43]). Briefly, the upstream and downstream flanking regions of the target genes, as well as the *lox66*-P_{32}*cat*-*lox71* cassette were amplified by PCR. The resulting amplicons were used as templates in a SOEing PCR reaction linking the flanking regions and *lox66*-P_{32}*cat*-*lox71* cassette together by means of complementary regions in the primers (Supplementary Table 1).

dx.doi.org/10.1021/cb1003509 |*ACS Chem. Biol.* 2011, 6, 366–376

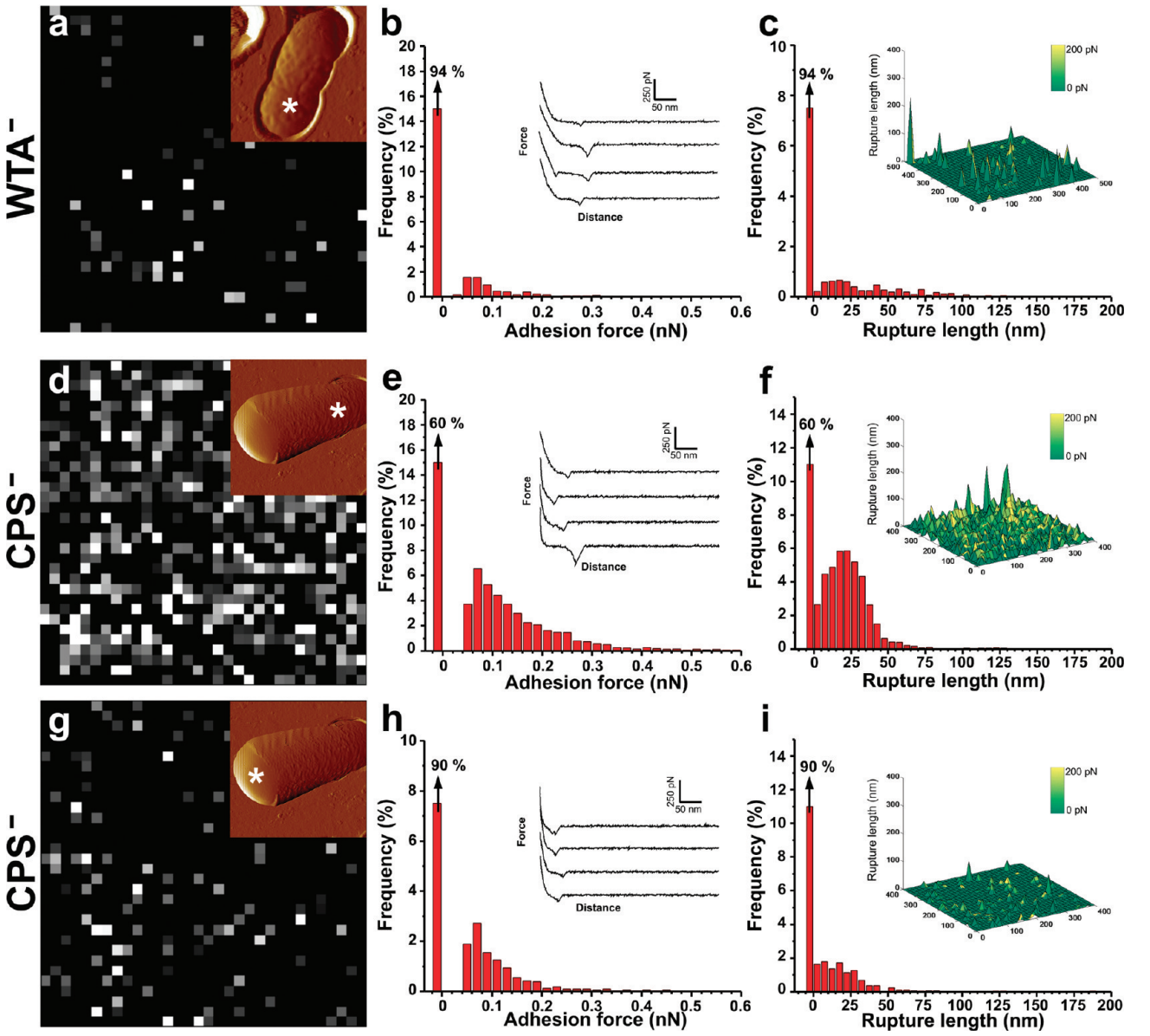

Figure 6. Single-molecule AFM imaging of WTAs in mutant cells. (a,d,g) Adhesion force map (500 × 500 nm, gray scale: 250 pN) recorded in buffer with a ConA tip on single WTA- (a) and single CPS- (d,g) deficient cells. Insets: deflection images in which the ∗ symbol indicates where the force maps were recorded. (b,e,h) Corresponding adhesion force histograms together with representative force curves. Each histogram was build from n = 4096 force curves from 4 maps, obtained using different tips and different cells. (c,f,i) Histograms of rupture distances and representative 3-D glycopolymer maps.

Subsequently, PCR products were cloned into SwaI-Ecl136II digested pNZ5319, an integration vector that does not replicate in *L. plantarum* or other Gram-positive hosts but can replicate in the intermediate cloning host *E. coli*.[43] The sequence of the cloned DNA fragment was confirmed by sequence analysis (BaseClear, Leiden, The Netherlands). The mutagenesis plasmids were transformed in *L. plantarum* WCFS1 and colonies displaying a chloramphenicol-resistant and erythromycin-sensitive phenotype, represent candidate double-cross over gene replacements. The anticipated *cat*-replacement genotype was confirmed by PCR using primers flanking the sites of recombination. This strategy was applied for the construction of *tagO::cat* (*lp_0730*; WTA-deficient strain, NZ3531Cm) and *cps4::cat* (*lp_2108* to *lp_2099*; NZ3534Cm) deletion mutants. In order to obtain the quadruple *cps1-4* mutant (CPS-deficient strain, NZ3534 + 3550Cm), the *lox66*-P_{32}*cat-lox71* cassette of the *cps4* mutant was excised by temporal expression of the *cre* recombinase using the unstable *cre* expression plasmid pNZ5348 as previously described.[43] The resulting *cps4::lox72* mutant (NZ3534) was used for a next round of mutagenesis targeting for the deletion of the region encompassing *cps1*, *cps2*, and *cps3* gene clusters (*lp_2108* to *lp_2099*) following the same procedures as described above.

Phenotype Analysis. For growth analysis, three independent cultures of the WT and WTA- and CPS-deficient strains were grown overnight in liquid MRS medium without addition of antibiotic. Overnight cultures were then diluted 1/100 in fresh medium, and growth was followed by measuring the $OD_{600\ nm}$ using a Varioskan Flash multimode reader (Thermo scientific) during 24 h. For cell morphology analysis, cells were harvested from cultures grown without antibiotic at early exponential and stationary growth phase, washed with PBS, and mounted on poly-L-lysin coated slides. Fluorescent staining of the membrane was achieved by adding FM4-64 (Invitrogen) to the cell sample (final

dx.doi.org/10.1021/cb1003509 |*ACS Chem. Biol.* 2011, 6, 366–376

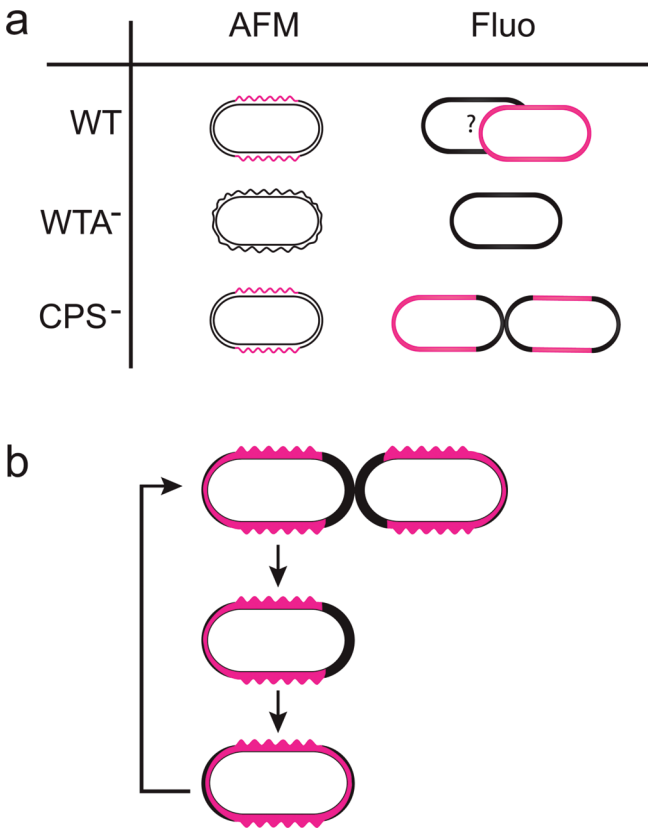

Figure 7. Spatial organization of WTAs in the *L. plantarum* cell wall: a dynamic three-dimensional view. (a) Schematic drawing of the cell wall of the WT and mutant strains. The cartoons emphasize the localization of glucose-based polymers as observed by single-molecule AFM (left; red color means glucose detection) and fluorescence microscopy (right; red color means glucose detection), as well as the cell surface nanomorphology (smooth *vs* rough) as observed by AFM imaging (left). (b) Integrated model for the localization and fate of WTAs during the cell cycle. According to the "inside to outside" mechanism of growth, the cell wall turnover is slower at the poles than in the longitudinal part of the cell. After cells separation, new material is progressively incorporated at the pole close to the plasma membrane, the older material being pushed toward the surface. Outer cell wall layers may therefore lack WTA (black, as observed by AFM), whereas inner layers would contain WTAs (red, as detected by fluorescence).

concentration of 5−10 μg/mL) just before the observation. Bright field and fluorescent images were acquired with a Hamamatsu ORCA-ER camera attached to a Leica DMR microscope. ImageJ (http://rsb.info.nih.gov/ij/) was used to analyze pictures; manipulation was limited to altering brightness and contrast. Scanning and transmission electron microscopy was performed as previously reported.[45]

Staining of Glycopolymers with Fluorescent ConA Lectin. Staining of glycopolymers was carried out on cells from exponentially growing and stationary phase cultures using the Alexa Fluor 594 conjugate of succinylated concanavalin A dimers (Alexa Fluor 594-ConA; Invitrogen). Cells were washed with 150 mM Na-acetate buffer (pH 4.7) and resuspended in 1 mL of the same buffer supplemented with Ca^{2+} and Mn^{2+} (1 mM) as cofactors. To test the specificity of the staining, a range of concentrations from 1 to 20 μg/mL of Alexa Fluor 594-ConA was then added, and the reactive mix was kept on ice for 30 min. Cells were washed with PBS and examined under the microscope as described above. Best results were obtained with 10 μg/mL of Alexa Fluor 594-ConA for the CPS-deficient strain and 1 μg/mL for the WT strain. As a control, WT cells were treated with TCA, which removes all polymers present at the cell surface. Cells (50 mL) were washed with 150 mM Na-acetate buffer (pH 4.7), resuspended in 10 mL, and boiled with 1 g of TCA during 10 min. TCA was removed by 3 washing steps with Na-acetate buffer, and cells were incubated with the ConA probe as described above.

X-ray Photoelectron Spectroscopy. WT and mutant cells were collected from exponentially growing cultures, resuspended in Milli-Q water (Millipore), and directly lyophilized. XPS analyses were performed on a Kratos Axis Ultra spectrometer (Kratos Analytical) equipped with a monochromatized aluminum X-ray source. The angle between the normal to the sample surface and the electrostatic lens axis was 0°. The analyzed area was ~700 × 300 μm. The constant pass energy of the hemispherical analyzer was set at 40 eV. The following sequence of spectra was recorded: survey spectrum, C_{1s}, N_{1s}, O_{1s}, P_{2p}, S_{2p} and C_{1s} again, to check the stability of charge compensation as a function of time and the absence of degradation of the sample during the analyses. To assess the level of surface contamination, sorbitol was included in the analyses, starting from the freeze-drying process. Binding energies were calculated with respect to the C-(C,H) component of the C1s peak of adventitious carbon fixed at 284.8 eV. Following subtraction of a linear baseline, molar fractions were calculated (CasaXPS program, Casa Software) using peak areas normalized on the basis of acquisition parameters, sensitivity factors and the transmission function provided by the manufacturer.

AFM Measurements. AFM images and force−distance curves were obtained in acetate buffer (150 mM in acetate, pH 4.75) at RT, using a Nanoscope V Multimode AFM (Veeco Metrology Group, Santa Barbara, CA). Cells were immobilized by mechanical trapping into porous polycarbonate membranes (Millipore, Billerica, MA) with a pore size similar to the bacterial cell size.[46] Before use, membranes were brought overnight at 110 °C and then cooled at RT. After filtering a cell culture, the filter was gently rinsed with the buffer, carefully cut (1 cm × 1 cm), and attached to a steel sample puck (Veeco Metrology Group) using a small piece of double face adhesive tape, and the mounted sample was transferred into the AFM liquid cell while avoiding dewetting. For imaging, MSCT tips (Veeco) were used taking care to minimize the applied force (<200 pN). For single-molecule force measurements, a cell was first localized using a bare tip, after which the tip was changed to a lectin-functionalized tip (see below). All force curves were recorded with MSCT tips at maximum applied force of ~350 pN with a loading rate of 17,000 pN/s. The spring constants of each cantilever were measured using the thermal noise method. Adhesion maps were obtained by recording 32 × 32 force−distance curves on areas of given size, calculating the adhesion force for each force curve and displaying the value as a gray pixel. To compare biopolymer properties on the different strains, three-dimensional reconstructed maps were obtained by combining adhesion force values (expressed as false colors) and rupture lengths (expressed as *z* level) measured at different *x*, *y* locations.

For single-molecule force measurements, AFM tips were functionalized with the Concavalin A lectin (ConA, Sigma) using PEG-benzaldehyde linkers as described by Ebner *et al.*[47] In our recording conditions (pH 4.75), the ConA tetramer dissociates into dimers. Cantilevers were washed with chloroform and ethanol, placed in an UV-ozone cleaner for 30 min, immersed overnight into an ethanolamine solution (3.3 g ethanolamine into 6 mL of DMSO), then washed 3 times with DMSO and 2 times with ethanol, and dried with N_2. The ethanolamine-coated cantilevers were immersed for 2 h in a solution prepared by mixing 1 mg of Acetal-PEG-NHS dissolved in 0.5 mL of chloroform with 10 μL of triethylamine, then washed with chloroform, and dried with N_2. Cantilevers were further immersed for 5 min in a 0.1% iodine/acetone solution, washed 3 times in acetone, dried under N_2, and then covered with a 200 μL droplet of a PBS solution containing ConA (0.2 mg/mL) to which 2 μL of a 1 M $NaCNBH_3$ solution was added. After 50 min, cantilevers were incubated with 5 μL of a 1 M ethanolamine solution

in order to passivate unreacted aldehyde groups and then washed with and stored in PBS 10 min later.

■ ASSOCIATED CONTENT

Supporting Information. This material is available free of charge *via* the Internet at http://pubs.acs.org.

■ AUTHOR INFORMATION

Corresponding Author

*yves.dufrene@uclouvain.be; pascal.hols@uclouvain.be

Author Contributions

#These authors contributed equally to this work

■ ACKNOWLEDGMENT

Work in the teams of Y.F.D. and P.H. was supported by the National Foundation for Scientific Research (FNRS), the Foundation for Training in Industrial and Agricultural Research (FRIA), the Université catholique de Louvain (Fonds Spéciaux de Recherche), the Federal Office for Scientific, Technical and Cultural Affairs (Interuniversity Poles of Attraction Programme), and the Research Department of the Communauté française de Belgique (Concerted Research Action). Y.F.D. and P.H. are Senior Research Associate and Research Associate of the FNRS. P.A.B is employed within the research programme of the Kluyver Centre for Genomics of Industrial Fermentation which is part of The Netherlands Genomics Initiative/Netherlands Organization for Scientific Research. We thank S. Derclaye, Y. Adriaensen, and M. Genet for helping us with the XPS analyses.

■ REFERENCES

(1) FAO, and WHO. (2001) Health and nutritional properties of probiotics in food including powder milk with live lactic acid bacteria, p 34, FAO, Rome/WHO, Geneva.

(2) Ahrné, S., Nobaek, S., Jeppsson, B., Adlerberth, I., Wold, A. E., and Molin, G. (1998) The normal *Lactobacillus* flora of healthy human rectal and oral mucosa. *J. Appl. Microbiol. 85*, 88–94.

(3) Vesa, T., Pochart, P., and Marteau, P. (2000) Pharmacokinetics of *Lactobacillus plantarum* NCIMB 8826, *Lactobacillus fermentum* KLD, and *Lactococcus lactis* MG 1363 in the human gastrointestinal tract. *Aliment. Pharmacol. Ther. 14*, 823–828.

(4) Adlerberth, I., Ahrne, S., Johansson, M., Molin, G., Hanson, L., and Wold, A. (1996) A mannose-specific adherence mechanism in *Lactobacillus plantarum* conferring binding to the human colonic cell line HT-29. *Appl. Environ. Microbiol. 62*, 2244–2251.

(5) Delcour, J., Ferain, T., Deghorain, M., Palumbo, E., and Hols, P. (1999) The biosynthesis and functionality of the cell wall of lactic acid bacteria. *Antonie van Leeuwenhoek 76*, 159–184.

(6) Neuhaus, F. C., and Baddiley, J. (2003) A continuum of anionic charge: structures and functions of D-alanyl-teichoic acids in Gram-positive bacteria. *Microbiol. Mol. Biol. Rev. 67*, 686–723.

(7) Weidenmaier, C., and Peschel, A. (2008) Teichoic acids and related cell-wall glycopolymers in Gram-positive physiology and host interactions. *Nat. Rev. Microbiol. 6*, 276–287.

(8) Baddiley, J., and Mathias, A. P. (1954) Cytidine nucleotides, Part I, isolation from *Lactobacillus arabinosus*. *J. Chem. Soc.* 2723–2731.

(9) Palumbo, E., Deghorain, M., Cocconcelli, P. S., Kleerebezem, M., Geyer, A., Hartung, T., Morath, S., and Hols, P. (2006) D-Alanyl ester depletion of teichoic acids in *Lactobacillus plantarum* results in a major modification of lipoteichoic acid composition and cell wall perforations at the septum mediated by the Acm2 autolysin. *J. Bacteriol. 188*, 3709–3715.

(10) Tomita, S., Irisawa, T., Tanaka, N., Nukada, T., Satoh, E., Uchimura, T., and Okada, S. (2010) Comparison of components and synthesis genes of cell wall teichoic acid among *Lactobacillus plantarum* strains. *Biosci. Biotechnol. Biochem. 74*, 928–933.

(11) Tomita, S., Furihata, K., Nukada, T., Satoh, E., Uchimura, T., and Okada, S. (2009) Structures of two monomeric units of teichoic acid prepared from the cell wall of *Lactobacillus plantarum* NRIC 1068. *Biosci. Biotechnol. Biochem. 73*, 530–535.

(12) Gründling, A., and Schneewind, O. (2007) Synthesis of glycerol phosphate lipoteichoic acid in *Staphylococcus aureus*. *Proc. Natl. Acad. Sci. U.S.A. 104*, 8478–8483.

(13) Grundling, A., and Schneewind, O. (2007) Genes required for glycolipid synthesis and lipoteichoic acid anchoring in *Staphylococcus aureus*. *J. Bacteriol. 189*, 2521–2530.

(14) Schirner, K., Marles-Wright, J., Lewis, R. J., and Errington, J. (2009) Distinct and essential morphogenic functions for wall- and lipo-teichoic acids in *Bacillus subtilis*. *EMBO J. 28*, 830–842.

(15) D'Elia, M. A., Millar, K. E., Beveridge, T. J., and Brown, E. D. (2006) Wall teichoic acid polymers are dispensable for cell viability in *Bacillus subtilis*. *J. Bacteriol. 188*, 8313–8316.

(16) D'Elia, M. A., Pereira, M. P., Chung, Y. S., Zhao, W., Chau, A., Kenney, T. J., Sulavik, M. C., Black, T. A., and Brown, E. D. (2006) Lesions in teichoic acid biosynthesis in *Staphylococcus aureus* lead to a lethal gain of function in the otherwise dispensable pathway. *J. Bacteriol. 188*, 4183–4189.

(17) Weidenmaier, C., Kokai-Kun, J. F., Kristian, S. A., Chanturiya, T., Kalbacher, H., Gross, M., Nicholson, G., Neumeister, B., Mond, J. J., and Peschel, A. (2004) Role of teichoic acids in *Staphylococcus aureus* nasal colonization, a major risk factor in nosocomial infections. *Nat. Med. 10*, 243–245.

(18) Oku, Y., Kurokawa, K., Matsuo, M., Yamada, S., Lee, B.-L., and Sekimizu, K. (2009) Pleiotropic roles of polyglycerolphosphate synthase of lipoteichoic acid in growth of *Staphylococcus aureus* cells. *J. Bacteriol. 191*, 141–151.

(19) Archibald, A. R., Armstrong, J. J., Baddiley, J., and Hay, J. B. (1961) Teichoic acids and the structure of bacterial walls. *Nature 191*, 570–572.

(20) Heptinstall, S., Archibald, A. R., and Baddiley, J. (1970) Teichoic acids and membrane function in bacteria. *Nature 225*, 519–521.

(21) Yamamoto, H., Miyake, Y., Hisaoka, M., Kurosawa, S. i., and Sekiguchi, J. (2008) The major and minor wall teichoic acids prevent the sidewall localization of vegetative dl-endopeptidase LytF in *Bacillus subtilis*. *Mol. Microbiol. 70*, 297–310.

(22) Schlag, M., Biswas, R., Krismer, B., Kohler, T., Zoll, S., Yu, W., Schwarz, H., Peschel, A., and Götz, F. (2010) Role of staphylococcal wall teichoic acid in targeting the major autolysin Atl. *Mol. Microbiol. 75*, 864–873.

(23) Eldholm, V., Johnsborg, O., Straume, D., Ohnstad, H. S., Berg, K. H., Hermoso, J. A., and Håvarstein, L. S. (2010) Pneumococcal CbpD is a murein hydrolase that requires a dual cell envelope binding specificity to kill target cells during fratricide. *Mol. Microbiol. 76*, 905–917.

(24) Dufrêne, Y. F., and Rouxhet, P. G. (1996) Surface composition, surface properties, and adhesiveness of *Azospirillum brasilense*—variation during growth. *Can. J. Microbiol. 42*, 548–556.

(25) Rouxhet, P. G., Mozes, N., Dengis, P. B., Dufrêne, Y. F., Gerin, P. A., and Genet, M. J. (1994) Application of X-ray photoelectron spectroscopy to microorganisms. *Colloids Surf. B. 2*, 347–369.

(26) Dufrêne, Y., van der Wal, A., Norde, W., and Rouxhet, P. (1997) X-ray photoelectron spectroscopy analysis of whole cells and isolated cell walls of gram-positive bacteria: comparison with biochemical analysis. *J. Bacteriol. 179*, 1023–1028.

(27) Andre, G., Kulakauskas, S., Chapot-Chartier, M.-P., Navet, B., Deghorain, M., Bernard, E., Hols, P., Dufrêne, Y. F. (2010) Imaging the nanoscale organization of peptidoglycan in living *Lactococcus lactis* cells, *Nat. Commun., 1*, doi: 10.1038/ncomms1027.

(28) Denis, F. A., Hanarp, P., Sutherland, D. S., Gold, J., Mustin, C., Rouxhet, P. G., and Dufrêne, Y. F. (2002) Protein adsorption on model

surfaces with controlled nanotopography and chemistry. *Langmuir 18*, 819–828.

(29) Francius, G., Lebeer, S., Alsteens, D., Wildling, L., Gruber, H. J., Hols, P., De Keersmaecker, S., Vanderleyden, J., and Dufrêne, Y. F. (2008) Detection, localization, and conformational analysis of single polysaccharide molecules on live bacteria. *ACS Nano 2*, 1921–1929.

(30) Mobley, H. L., Koch, A. L., Doyle, R. J., and Streips, U. N. (1984) Insertion and fate of the cell wall in *Bacillus subtilis*. *J. Bacteriol. 158*, 169–179.

(31) Umeda, A., Yokoyama, S., Arizono, T., and Amako, K. (1992) Location of peptidoglycan and teichoic acid on the cell wall surface of *Staphylococcus aureus* as determined by immunoelectron microscopy. *J. Electron Microsc. 41*, 46–52.

(32) Hinterdorfer, P., and Dufrêne, Y. F. (2006) Detection and localization of single molecular recognition events using atomic force microscopy. *Nat. Methods 3*, 347–355.

(33) Dufrêne, Y. F. (2008) Towards nanomicrobiology using atomic force microscopy. *Nat. Rev. Microbiol. 6*, 674–680.

(34) Müller, D. J., Helenius, J., Alsteens, D., and Dufrêne, Y. F. (2009) Force probing surfaces of living cells to molecular resolution. *Nat. Chem. Biol. 5*, 383–390.

(35) Alsteens, D., Dupres, V., Mc Evoy, K., Wildling, L., Gruber, H. J., and Dufrêne, Y. F. (2008) Structure, cell wall elasticity and polysaccharide properties of living yeast cells, as probed by AFM. *Nanotechnology 19*, 384005.

(36) Francius, G., Alsteens, D., Dupres, V., Lebeer, S., De Keersmaecker, S., Vanderleyden, J., Gruber, H. J., and Dufrêne, Y. F. (2009) Stretching polysaccharides on live cells using single molecule force spectroscopy. *Nat. Protoc. 4*, 939–946.

(37) Holtje, J. V. (1998) Growth of the stress-bearing and shape-maintaining murein sacculus of *Escherichia coli*. *Microbiol. Mol. Biol. Rev. 62*, 181–203.

(38) Koch, A. L., and Doyle, R. J. (1985) Inside-to-outside growth and turnover of the wall of gram-positive rods. *J. Theor. Biol. 117*, 137–157.

(39) Atilano, M. L., Pereira, P. M., Yates, J., Reed, P., Veiga, H., Pinho, M. G., and Filipe, S. R. (2010) Teichoic acids are temporal and spatial regulators of peptidoglycan cross-linking in *Staphylococcus aureus*. *Proc. Natl. Acad. Sci. U.S.A. 107*, 18991–18996.

(40) Campbell, J., Singh, A. K., Santa Maria, J. P., Kim, Y., Brown, S., Swoboda, J. G., Mylonakis, E., Wilkinson, B. J., and Walker, S. (2010) Synthetic lethal compound combinations reveal a fundamental connection between wall teichoic acid and peptidoglycan biosyntheses in *Staphylococcus aureus*. *ACS Chem. Biol.*in press.

(41) Kleerebezem, M., Boekhorst, J., van Kranenburg, R., Molenaar, D., Kuipers, O. P., Leer, R., Tarchini, R., Peters, S. A., Sandbrink, H. M., Fiers, M. W. E. J., Stiekema, W., Lankhorst, R. M. K., Bron, P. A., Hoffer, S. M., Groot, M. N. N., Kerkhoven, R., de Vries, M., Ursing, B., de Vos, W. M., and Siezen, R. J. (2003) Complete genome sequence of *Lactobacillus plantarum* WCFS1. *Proc. Natl. Acad. Sci. U.S.A. 100*, 1990–1995.

(42) Sambrook, J., Fritsch, E. F., Maniatis, T. (1989) *Molecular Cloning: A Laboratory Manual*, 2nd ed., Cold Spring Harbor, New York.

(43) Lambert, J. M., Bongers, R. S., and Kleerebezem, M. (2007) Cre-lox-based system for multiple gene deletions and selectable-marker removal in *Lactobacillus plantarum*. *Appl. Environ. Microbiol. 73*, 1126–1135.

(44) Meijerink, M., van Hemert, S., Taverne, N., Wels, M., de Vos, P., Bron, P. A., Savelkoul, H. F., van Bilsen, J., Kleerebezem, M., and Wells, J. M. (2010) Identification of genetic loci in *Lactobacillus plantarum* that modulate the immune response of dendritic cells using comparative genome hybridization. *PLoS ONE 5*, e10632.

(45) Palumbo, E., Favier, C. F., Deghorain, M., Cocconcelli, P. S., Grangette, C., Mercenier, A., Vaughan, E. E., and Hols, P. (2004) Knockout of the alanine racemase gene in *Lactobacillus plantarum* results in septation defects and cell wall perforation. *FEMS Microbiol. Lett. 233*, 131–138.

(46) Dufrêne, Y. F. (2008) Atomic force microscopy and chemical force microscopy of microbial cells. *Nat. Protoc. 3*, 1132–1138.

(47) Ebner, A., Wildling, L., Kamruzzahan, A. S. M., Rankl, C., Wruss, J., Hahn, C. D., Holzl, M., Zhu, R., Kienberger, F., Blaas, D., Hinterdorfer, P., and Gruber, H. J. (2007) A new, simple method for linking of antibodies to atomic force microscopy tips. *Bioconjugate Chem. 18*, 1176–1184.